Journal of *Marine Science and Engineering*

MDPI

Article

Calibration Procedures for NO_x Emissions Model of a High-Speed Marine Diesel Engine Using Optimization Procedures

Mina Tadros [1,2,*] and Evangelos Boulougouris [1]

[1] Department of Naval Architecture, Ocean and Marine Engineering, Maritime Safety Research Centre (MSRC), University of Strathclyde, Glasgow G4 0LZ, UK; evangelos.boulougouris@strath.ac.uk
[2] Department of Naval Architecture and Marine Engineering, Faculty of Engineering, Alexandria University, Alexandria 21544, Egypt
* Correspondence: mina.tadros@strath.ac.uk

Abstract

Controlling nitrogen oxide (NO_x) emissions is a critical priority for the maritime industry, driven by increasingly stringent international maritime organization (IMO) Tier III regulations and the sector's broader decarbonization efforts. Accurate prediction and minimization of NO_x emissions require well-calibrated engine models that reflect real-world operating behavior under varied conditions. This study presents a robust calibration methodology for the NO_x emissions model of a high-speed dual-fuel marine engine, using a 1D engine simulation platform (WAVE 2025.1) integrated with a nonlinear optimization algorithm (fmincon in MATLAB R2025a). The calibration focuses on tuning the extended Zeldovich mechanism by empirically adjusting the Arrhenius equation coefficients to achieve a weighted sum of NO_x and unburned hydrocarbon (HC) emissions below the 7.2 g/kWh regulatory threshold. The proposed approach reduces the need for extensive experimental data while maintaining high predictive accuracy. Simulation results confirm compliance with IMO regulations across multiple engine loads defined by the E3 test cycle. A sensitivity analysis further revealed that while the pre-exponent multiplier (ARC1) plays a critical role in influencing NO_x emissions at high loads, the exponent multiplier (AERC1) has an even more significant impact across the full load range, making its precise calibration essential for robust emissions modeling. The calibrated NO_x emissions model not only ensures realistic emissions estimation but also provides a reliable foundation for further research, such as dual-fuel performance studies, and can be effectively integrated into future engine optimization tasks under different operating conditions.

Keywords: NO_x emissions; 1D engine model; optimization procedures; marine engine; Zeldovich mechanism

check for updates

Academic Editors: Elias Yfantis, Theodoros Zannis and George Mallouppas

Received: 13 July 2025
Revised: 15 August 2025
Accepted: 18 August 2025
Published: 19 August 2025

Citation: Tadros, M.; Boulougouris, E. Calibration Procedures for NO_x Emissions Model of a High-Speed Marine Diesel Engine Using Optimization Procedures. *J. Mar. Sci. Eng.* **2025**, *13*, 1585. https://doi.org/10.3390/jmse13081585

Copyright: © 2025 by the authors. Licensee MDPI, Basel, Switzerland. This article is an open access article distributed under the terms and conditions of the Creative Commons Attribution (CC BY) license (https://creativecommons.org/licenses/by/4.0/).

1. Introduction

The International Maritime Organization (IMO) is making significant efforts to reduce exhaust emissions from ships, aligning with global strategies to achieve net-zero greenhouse gas (GHG) emissions by 2050. Both short-term and long-term measures have been introduced to accelerate the transition towards climate neutrality within the proposed timeframe [1].

In the short term, research and industry practices have focused on improving the energy efficiency of conventional diesel engines through modifications and real-time op-

timization [2]. Several studies have explored the role of engine tuning and combustion control as effective strategies for reducing brake specific fuel consumption (BSFC) [3–6]. For example, adjustments to injection timing [7–10], exhaust gas recirculation (EGR) [11–14], and turbocharging [15,16] have demonstrated measurable improvements in engine thermal efficiency and emissions control.

In contrast, long-term decarbonization requires a paradigm shift in marine fuel and engine technologies [17]. A growing body of research is focused on the development and integration of low- and zero-carbon fuels such as liquefied natural gas (LNG), methanol, biofuels, ammonia, and hydrogen [1,18–20]. Each alternative presents unique opportunities and challenges in terms of energy density, emissions profile, combustion characteristics, and infrastructure requirements. For instance, LNG adoption has increased due to its lower carbon dioxide (CO_2) and sulfur oxides (SO_x) emissions, although concerns persist regarding methane slip. Methanol, particularly when produced from renewable sources, is gaining attention for its ease of handling and lower pollutant formation [21–23].

Several manufacturers and research initiatives have developed dual-fuel engines capable of operating on both conventional marine diesel and alternative fuels. These engines offer a transitional solution, enabling the gradual integration of cleaner fuels while maintaining compatibility with existing bunkering infrastructure [24,25].

One key strategy is optimizing dual-fuel engine performance across the engine load diagram, enabling ships to operate at lower fuel consumption levels in both liquid and gas modes. This approach not only enhances energy efficiency but also significantly reduces exhaust emissions. Another critical solution lies in the exploration and adoption of alternative fuels. Utilizing innovative fuel options provides operational flexibility, allowing ships to adjust performance along their routes while maintaining tighter control over emissions [18,24,26,27]. Together, these strategies support the maritime sector's transition to cleaner, more sustainable operations. As the maritime sector adopts alternative fuels, it not only curbs CO_2 emissions but also moves closer to achieving lower levels of Nitrogen oxides (NO_x) emissions, as suggested by the international regulators, as in Figure 1.

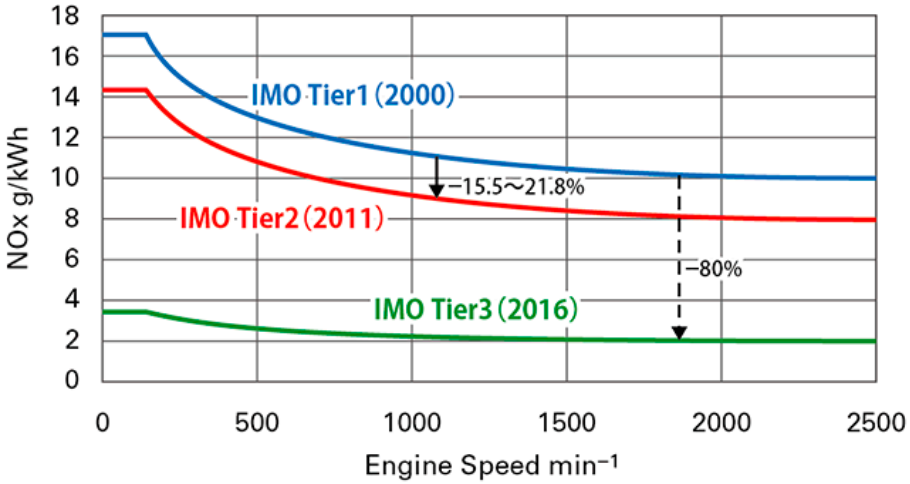

Figure 1. NO_x emission limits for marine engines [24].

NO_x emissions are a significant environmental concern in the maritime industry due to their contribution to air pollution and the adverse health effects they cause. Reducing NO_x emissions has become a priority under international regulations such as the IMO Tier standards, which mandate stringent vessel limits [28]. The transition to new fuels plays an essential role in reducing NO_x emissions. Fuels such as hydrogen, ammonia, and some biofuels offer cleaner combustion profiles, often resulting in lower NO_x output compared to traditional marine diesel oil (MDO) or heavy fuel oil (HFO) [29,30].

While nitric oxide (NO) and nitrogen dioxide (NO_2) are considered NO_x emissions, NO is the dominant nitrogen oxide formed within the engine cylinder during combustion. This predominance arises because NO is primarily generated through high-temperature reactions between nitrogen (N_2) and oxygen (O_2) in the air, as described by the Zeldovich mechanism [31], which has been widely used to compute NO_x emissions [32–35]. The extreme heat of the combustion process provides the energy needed to break the strong triple bond in nitrogen molecules, allowing them to react with oxygen to form NO. NO_2 is typically formed in smaller quantities and often results from the oxidation of NO as it cools and interacts with residual oxygen in the exhaust system. Several factors, including combustion temperature, air-fuel mixture, and post-combustion exhaust treatment systems, can influence the balance between NO and NO_2 concentrations. Understanding the formation dynamics of NO as the primary NO_x component is crucial for developing strategies to mitigate overall NO_x emissions and comply with increasingly stringent environmental regulations. The three primary reactions in the extended Zeldovich mechanism are:

$$O + N_2 \leftrightarrow NO + N \quad (1)$$

$$N + O_2 \leftrightarrow NO + O \quad (2)$$

$$N + OH \leftrightarrow NO + H \quad (3)$$

where O, N and H are oxygen, nitrogen and hydrogen atoms.

The formation of NO_x is highly temperature-dependent, increasing exponentially at temperatures above 2000 degrees Kelvin. Factors such as combustion temperature, oxygen concentration, residence time of reactants in the high-temperature zone, and local air-fuel equivalence ratio play a critical role in determining the rate of NO_x formation [31].

The recent literature explores a broad spectrum of methodologies aimed at understanding and reducing NO_x emissions, leveraging both experimental studies and numerical simulations to assess combustion dynamics, fuel interactions, and emission characteristics under varied operating conditions.

NO_x emissions calculations in engine simulation models are essential for predicting and optimizing the environmental performance of marine engines. These models leverage detailed thermodynamic and chemical kinetics data to simulate the combustion process and the subsequent formation of NO_x. The NO_x emissions are calculated based on the Zeldovich mechanism, which describes the thermal formation of NO_x as a function of temperature, oxygen concentration, and residence time in high-temperature zones. These calculations are particularly useful for evaluating the impact of both fossil and alternative fuels, such as hydrogen or ammonia, which have distinct combustion characteristics. By simulating engine performance across the load range, engine models help identify optimal operating parameters to minimize NO_x emissions while maintaining efficiency, supporting compliance with IMO regulations, and advancing sustainable maritime practices.

The simulation of NO_x emissions is carried out progressively, starting from 1D models and advancing to more detailed 3D engine models, depending on the level of detail available in the combustion process. In 1D models, the combustion chamber is typically divided into two primary zones: the burned and unburned regions. This two-zone approach is widely used due to its computational efficiency and ability to provide reliable predictions of NO_x formation under various operating conditions. However, as the complexity of the model increases, such as in 3D simulations, additional zones can be defined to capture more intricate phenomena [36,37]. High-dimensional models allow for a more precise representation of temperature gradients, chemical species distribution, and flow dynamics within the combustion chamber, making them particularly suitable for advanced studies of NO_x formation and mitigation strategies.

A major focus across several studies is the application of computational fluid dynamics (CFD) to simulate combustion and the formation of NO_x. Multiple studies have utilized CFD tools to optimize fuel injection strategies, analyze in-cylinder temperature fields, and assess the impact of piston bowl geometry and swirl ratios on NO_x emissions. These simulations provide granular insight into the thermodynamic behavior of combustion, revealing that strategic control of ignition delay and injection phasing can significantly reduce peak flame temperatures, thereby suppressing NO_x formation. These number of works incorporated experimental investigations to validate simulation models and assess the performance of marine engines under various fuel strategies.

Studies presented by Cuper-Przybylska et al. [38] and Jo et al. [39] developed detailed 3D CFD models covering full engine cycles. These models, validated against experimental data, provide accurate predictions of in-cylinder pressure and emissions, with mean errors of less than 1.5% for NO_x and pressure profiles. The modeling incorporates advanced turbulence (k-ε RNG), spray breakup, and NO_x formation mechanisms (extended Zeldovich), demonstrating robust predictive capabilities. Similarly, Sun et al. [40] and Lamas and Rodríguez [41] compared simulations with experimental measurements under various load and fuel conditions, reinforcing the reliability of integrated modeling–measurement methodologies. The computation is based on different dimensional models to simulate combustion processes of heavy fuel oil in medium-speed engines, and a strong correlation between simulation and actual NO_x, carbon monoxide (CO), and particulate matter (PM) values has been found.

Şener and Gül [42] utilized a refined numerical approach to optimize the combustion chamber geometry and injection parameters in marine diesel engines, demonstrating how computational models can significantly influence the design of low-emission systems. Karvounis et al. [43] conducted a parametric study to investigate the impact of methanol percentage on the combustion behavior and NO_x formation in a dual-fuel engine. Liu et al. [44] numerically investigated ammonia–diesel co-combustion and found substantial NO_x reductions reaching the Tier 2 limits.

In addition to the computational findings validated through experimental testing, the integration of machine learning (ML) techniques has emerged as a promising advancement for enhancing real-time NO_x prediction models during actual ship operations. These models utilize high-resolution operational data collected from on-board sensors, including engine speed, load, ambient conditions, and fuel injection parameters, to predict NO_x emissions dynamically and accurately. By continuously learning from sensor inputs across various voyage scenarios, ML-based models can adapt to changes in operational profiles and environmental factors, offering superior flexibility compared to static physics-based approaches. Moreover, the development of simplified surrogate models—trained on data from both CFD simulations and experimental campaigns—has proven effective in capturing the influence of key variables such as injection timing, pressure, and fuel composition on NO_x formation. These models are increasingly recommended for practical implementation in digital twins or real-time monitoring platforms, enabling operators to optimize engine performance and comply with stringent emission regulations like IMO Tier III and regional emission control area (ECA) standards [32,45,46].

Collectively, the reviewed body of work underscores the interdisciplinary nature of NO_x prediction and reduction research in marine engines. Experimental approaches provide essential validation and insights into real-world emission behaviors, while numerical simulations extend the design and analysis scope beyond practical test limits. Meanwhile, artificial intelligence (AI) and data-driven models offer real-time predictive control opportunities, and alternative fuels present a pathway toward long-term decarbonization with co-benefits for NO_x mitigation [47–49]. This integrated framework is essential for

guiding the development of next-generation marine propulsion systems that are both environmentally compliant and operationally efficient.

Despite the increasing fidelity of modeling techniques, calibrating NO_x emissions models—especially in 1D engine simulation platforms—remains a significant challenge. Achieving accurate NO_x predictions typically requires detailed experimental data at each operating point, owing to the sensitivity of thermal NO_x formation to local temperature and pressure conditions. This extensive calibration process is time-consuming and resource-intensive, often limiting the practical deployment of 1D predictive models for emissions in early design phases.

To address this gap, the present work proposes a simplified, yet effective NO_x emissions prediction approach based on the overall NO_x characteristics in g/kWh available in engine manufacturer project guides or technical documentation. This reference average data forms the empirical basis for model calibration and is used to generate an approximate emissions map.

Rather than attempting to model NO_x formation through detailed chemical kinetics or exhaust measurements at every operating point, the proposed method aggregates NO_x and HC formation into a single empirical emission map. This map is derived from the total emissions stated by the manufacturer and reflects an integrated view of combustion characteristics across the engine's operational envelope. The approach reduces dependency on high-resolution calibration while maintaining acceptable accuracy for comparative studies and early-stage design assessments, particularly valuable in dual-fuel and clean-fuel retrofit evaluations.

2. Engine Specifications

The marine dual-fuel engine analyzed in this study is the MAN D2862 LE448 [50], a high-performance, high-speed engine designed for marine applications. This engine is a modified version of the original marine diesel engine, the MAN D2862 LE428, and has been adapted to operate in dual-fuel mode. It functions in two distinct modes: liquid mode, using MDO as fuel, and gas mode, where hydrogen serves as the primary injection fuel. The engine is equipped with a common rail fuel injection system, enabling precise control of injection timing and pressure. Additionally, it incorporates an exhaust gas turbocharging system with twin turbochargers and a wastegate for improved air management and charge efficiency. It is well-suited for installation on fast workboats and small tugboats, offering a sustainable solution for marine propulsion that complies with IMO Tier 3 emissions standards through the integration of a selective catalytic reduction (SCR) system.

The engine operates under atmospheric intake conditions, with intake pressure and temperature set at 100 kPa and 318 K, respectively, and can generate a maximum power output of 749 kW at 2100 rpm. With its dual-fuel capability, the MAN D2862 LE448 supports efforts to reduce greenhouse gas emissions in the maritime sector while maintaining high power output and operational flexibility. Table 1 shows the main characteristics of the selected engine.

Table 1. Main engine specifications [51].

Item	Unit	Value
Bore	mm	128
Stroke	mm	157
No. of cylinders	-	12
Displacement	L	24.24
Number of valves per cylinder	-	4

Table 1. *Cont.*

Item	Unit	Value
Compression ratio	-	19:1
Brake mean effective pressure	bar	17.66
Piston speed	m/s	10.99
Engine speed	rpm	2100
Brake Specific fuel consumption	g/kWh	208
Power-to-weight ratio	kW/kg	0.329

3. Engine Optimization Model

The developed engine optimization model presented in this study is shown in Figure 2. The proposed optimization model integrates WAVE 2025.1 [52], a 1D engine simulation software, with a nonlinear optimization algorithm (fmincon) implemented in MATLAB R2025a [53]. This model is developed to fine-tune the extended Zeldovich mechanism, in particular the pre-exponent multiplier and exponent multiplier, to achieve a targeted weighted value of NO_x and HC emissions with a maximum value of 7.2 g/kWh, as commonly required for marine diesel engines according to the collected data [54]. The weighted values of the summation of both types of exhaust emissions are computed according to the test cycle E3, where four operating points at different engine power and speed are considered, as presented in Table 2. Direct experimental NO_x measurements at multiple load points are not available for the present study. Instead, NO_x emission characteristics are taken from the manufacturer's technical documentation, which is used as a reference target for the calibration process.

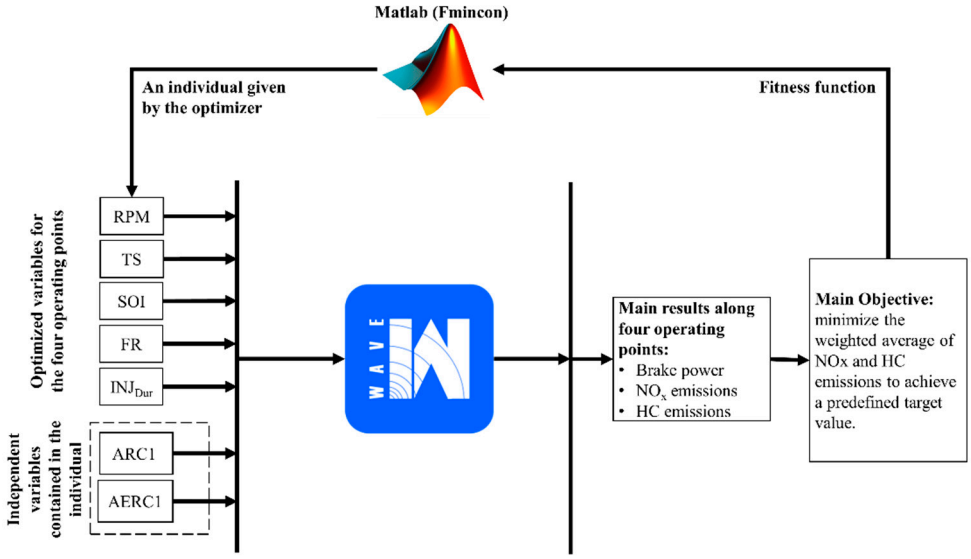

Figure 2. Schematic diagram of the engine optimization model.

Table 2. Test cycle E3 for propeller law-operated main engines [55].

Engine speed (RPM)	100%	91%	80%	63%
Engine brake power (P_B)	100%	75%	50%	25%
Weighting factor (w)	0.2	0.5	0.15	0.15

Before performing the calibration procedure of the NO_x emission model, the engine model is built in WAVE and undergoes a comprehensive optimization process, following the methodology proposed by Tadros [56]. This approach emphasizes the integration of a

friction model within the overall engine optimization framework to improve simulation fidelity and performance prediction. The friction losses have been evaluated using a custom-built friction fitting tool developed in Excel, which was coupled with the engine performance model. The tool utilizes the Chen-Flynn correlation [57], a widely recognized empirical model for estimating engine friction mean effective pressure (FMEP), and the correlation parameters have been meticulously optimized to align with measured data, thereby enhancing the accuracy of the simulation results across the entire operating range.

Once the friction model has been validated and the Chen-Flynn parameters have been optimized, these values are implemented into the engine performance model to reflect the friction equation. The same optimization concept is then extended to evaluate engine behavior at each operating point. The optimization routine aimed to maximize the air-fuel ratio (AFR) within thermodynamic constraints, such as maximum allowable in-cylinder pressure and temperature, while ensuring a specific target brake power output. Key control parameters, including turbocharger speed (TS), start of injection (SOI), and injection duration (Inj_{Dur}), are iteratively adjusted to find the optimal combination that meets the performance targets. The turbocharger model is defined to operate at a constant speed, allowing TS to be treated as a key control parameter within the optimization framework. This option is allowed in the WAVE software and is preferred when turbocharger maps are scaled from existing maps, as it provides a practical means of adjusting compressor behavior without requiring detailed actuator modeling. Additionally, a simple controller regulates the wastegate valve based on the maximum allowed intake manifold pressure to ensure the safety of the engine. As the engine features a common rail system, rail pressure is a potential future control parameter for optimization, although it was held constant in this study.

Importantly, the combustion process is analyzed across all three phases, ignition delay, premixed combustion, and diffusion combustion, to ensure stable and efficient combustion throughout the engine's operating map [58,59]. This robust optimization strategy provided a well-calibrated foundation for the subsequent NO_x emission modeling, ensuring that the engine operated under realistic and physically consistent conditions.

After completing the optimization procedures at the four previously defined operating points, the NO_x and HC emission models are activated within WAVE to enable the prediction of key emission species across a range of engine loads. This step marks a crucial transition from performance-focused modeling to environmental evaluation, ensuring that the engine operates not only efficiently but also within regulatory emission limits.

The NO_x emission model in WAVE plays a vital role in accurately predicting the environmental behavior of internal combustion engines under diverse operating conditions. In this study, NO_x emissions are modeled using the extended Zeldovich mechanism [31], which serves as the foundation of WAVE's semi-predictive NO_x model. This mechanism simulates the thermal formation of NO, the dominant NO_x species, through high-temperature reactions between molecular nitrogen and oxygen during the combustion process. As a result, the model is highly sensitive to critical in-cylinder parameters such as peak combustion temperature, pressure, oxygen concentration, and residence time of reactants.

Due to this sensitivity, the NO_x model must be embedded within a well-calibrated and physically consistent engine model, which is why the optimization of engine performance and combustion stability is performed prior to emissions analysis. This integration enables the accurate simulation of NO_x emissions across various loads and operating conditions. By using the calibrated model, the NO_x predictions accurately reflect realistic trends, enabling further investigation into emissions mitigation strategies, including injection timing optimization, turbocharger control, and dual-fuel ratio adjustments.

Based on the extended Zeldovich mechanism, NO_x emissions are calculated using the predefined reaction rate equations embedded within the emissions module of WAVE. Each reaction follows an Arrhenius-type expression, where the formation rate is governed by a specific rate constant defined by a pre-exponential factor and a temperature-dependent exponential term. These rate constants correspond to the key reactions in the mechanism—namely the formation of NO through the thermal reactions between nitrogen and oxygen species—and are parameterized using the Arrhenius coefficients (ARC1 and AERC1) for calibration purposes, as shown in the following expressions:

$$R_1 = A \times ARC1 \times e^{\left(\frac{T_a \times AERC1}{T}\right)} \quad (4)$$

$$R_{2,3} = A \times e^{\left(\frac{T_a}{T}\right)} \quad (5)$$

where A is the pre-exponential constant, ARC1 is the user-entered pre-exponent multiplier, T_a is the activation temperature for the reaction, AERC1 is the user-entered exponent multiplier, and T is the burned-zone temperature.

The HC emissions sub-model in WAVE estimates HC emissions within an engine cylinder element based on a simplified correlation that considers the injector's sac volume. This sub-model is specifically designed for direct-injected engines and does not require the engine cylinder element to be configured with the two burning and unburning zones, simplifying its implementation in single-zone combustion simulations.

The model assumes that a fraction of the fuel remaining in the injector sac volume contributes directly to HC emissions due to incomplete combustion. The fraction of the injector sac volume contributing to unburned hydrocarbons is a user-defined parameter, with a recommended default value of 0.2. Accurate prediction of HC emissions using this sub-model requires that the sac volume is properly specified in the corresponding injector element within the model architecture.

In the current study, the available manufacturer documentation provided aggregated emission characteristics rather than detailed NO_x measurements for each load point. While the HC sub-model in WAVE is simplified and based on injector sac volume, HC levels are consistently less than 2% of the total NO_x + HC value, making their influence on NO_x coefficient calibration negligible.

Once the computation of engine performance is performed over multiple operating points (n), the weighted average of NO_x and HC emissions is calculated using the following general equation:

$$Emissions_{Type} = \frac{\sum_{i=1}^{n} (Emissions_{flow,i}.w_i)}{\sum_{i=1}^{n} (P_{B,i}.w_i)} \quad (6)$$

The optimization model employed in this study is based on the fmincon algorithm, a local optimization solver in MATLAB R2025a designed to minimize constrained nonlinear multivariable functions [53]. The selection of fmincon is motivated by its computational efficiency and robustness in handling complex engineering problems with nonlinear constraints. Unlike global optimization algorithms, which often require significantly more computational time and may not guarantee convergence within practical limits, fmincon offers a reliable trade-off between solution accuracy and computational speed. This makes it particularly suitable for iterative engine calibration or control parameter tuning tasks, where a prompt response is essential.

The boundary conditions for the control parameters ARC1 and AERC1 are defined within the range of 0.8 to 1.2. The fitness function, denoted as f, is evaluated using the following expression, which quantitatively assesses the deviation between the predicted and target

engine performance metrics under given operating conditions. This formulation enables efficient convergence of the optimization algorithm by penalizing deviations from desired outcomes, thereby guiding the search toward the optimal set of control parameter values.

$$f = \left| \frac{\text{Calculated}_{\text{NOx+HC}}}{\text{Target}_{\text{NOx+HC}}} - 1 \right| \quad (7)$$

where the $\text{Calculated}_{\text{NOx+HC}}$ is computed from the summation of the two types of exhaust emissions based on Equation (6), while the $\text{Target}_{\text{NOx+HC}}$ is equal to 7.2 based on the real data.

4. Results

4.1. Optimization of the NO_x Emissions Model

To provide a comprehensive understanding of the engine optimization process, particularly during the calibration of FMEP and NO_x emissions, a schematic representation of the integrated optimization framework is illustrated in Figure 3. This diagram illustrates the structural interaction between the main engine performance model and its integration with two key sub-models: the friction loss estimation based on the Chen-Flynn correlation and the NO_x emissions prediction model. Specifically, the engine model is adapted to optimize the parameters of the Chen-Flynn empirical correlation, enabling accurate estimation of FMEP under varying operating conditions. Simultaneously, the model incorporates a NO_x emissions optimization module, which focuses on calibrating the Arrhenius equations to predict NO_x formation with high fidelity. By coupling these two subsystems with the core engine simulation, the optimization framework allows for the concurrent refinement of control parameters—such as injection timing, duration, and turbocharger speed—while ensuring compliance with both performance targets and emission regulations. This integrated structure enhances the predictive capability of the model and ensures a realistic, multi-objective optimization process aligned with real engine behavior and regulatory standards.

After defining the values of Chen-Flynn correlation, the performance of the engine model is optimized at four representative operating points defined by the NO_x Technical Code, as outlined in Table 2. The optimization framework is capable of predicting the optimal values for key control parameters, namely turbocharger speed, fuel injection rate, SOI, and injection duration, with the primary objective of maximizing the AFR, while ensuring compliance with thermodynamic constraints and maintaining combustion stability, as described by Tadros [56]. The optimization results are illustrated in Figure 4, presented in a normalized form relative to Case (1), which corresponds to the engine's rated operating condition. As observed, both turbocharger speed and fuel injection rate decrease with the reduction in engine load. A significant shift in SOI is also evident, with values ranging between -1.5 and -3.6 degree before top dead center (BTDC), indicating a tendency to advance injection timing at the different loads before the piston reaches the TDC. In contrast, injection duration shows an increasing trend as engine load decreases, reflecting the need for longer fuel delivery periods to sustain combustion under reduced thermal input conditions. The variation in values along the different load points suggests an active role of air and fuel management strategies in improving the AFR, thus the combustion and pressure behavior change inside the cylinder, reducing the exhaust emissions.

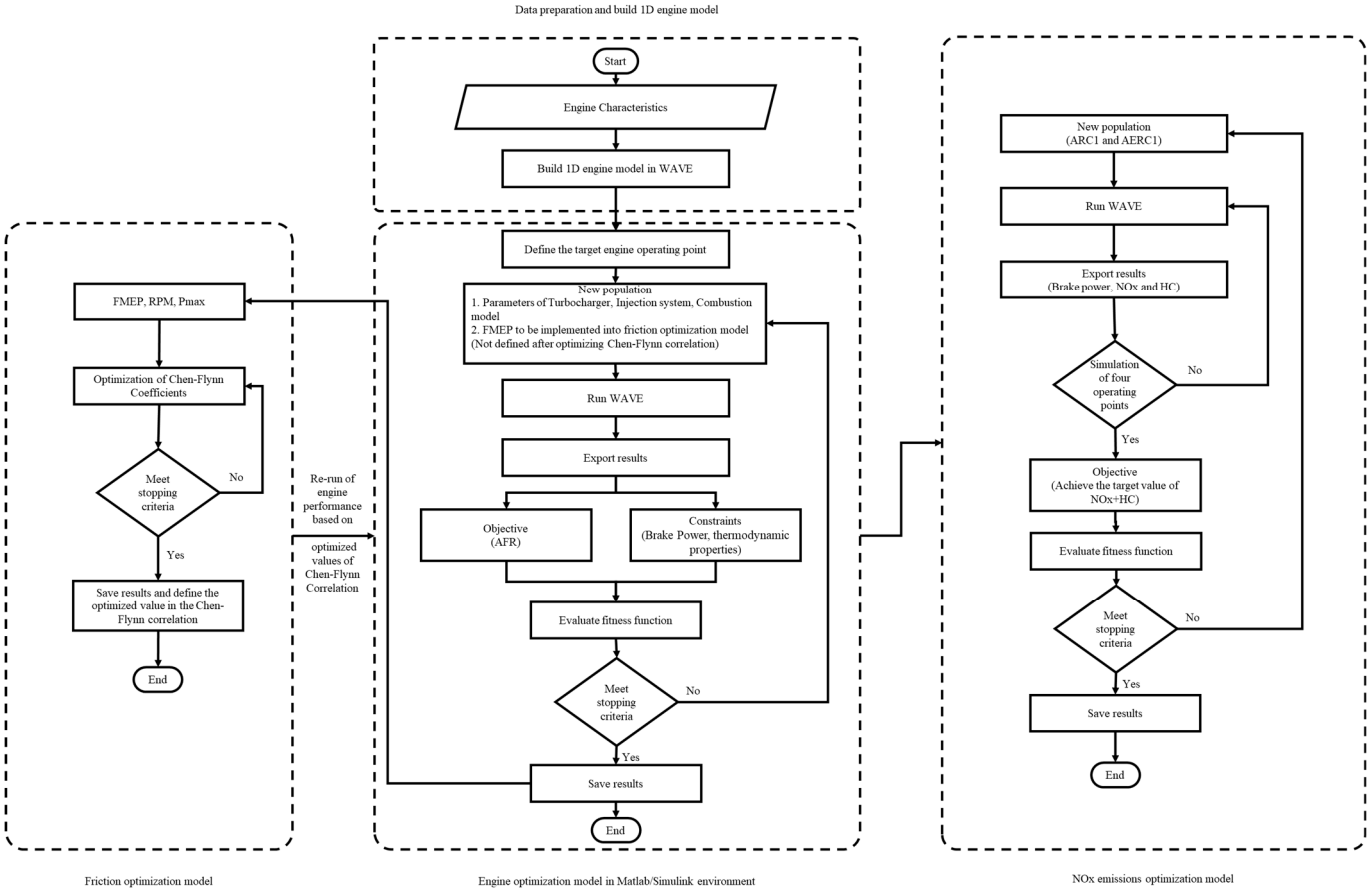

Figure 3. Schematic diagram of the framework of the engine optimization model.

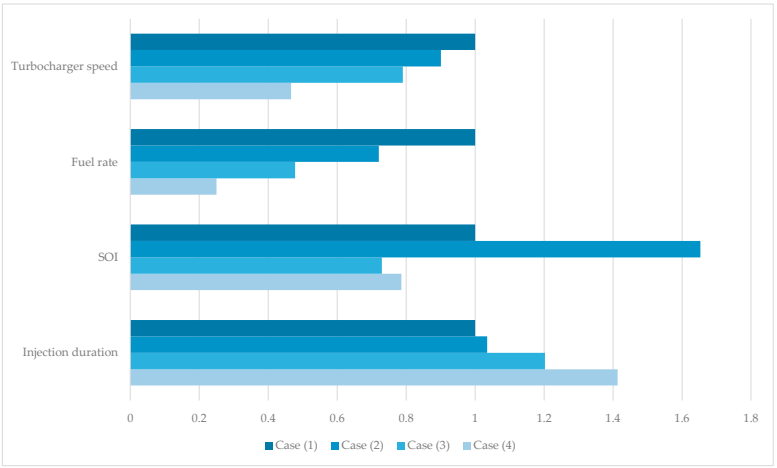

Figure 4. Variation in normalized engine characteristics at different engine operating points.

4.2. Results of Optimization

Once the four operating points are optimized, the NO_x emissions optimization is developed to find the optimal solution of the parameters of Arrhenius equations. The standard procedure of the optimization model begins by defining the objective function to achieve the summation of the weighted average of NO_x and HC. The decision variables are then bounded within operationally feasible ranges, and the optimization problem is solved iteratively using a constrained nonlinear optimization algorithm (e.g., fmincon in MATLAB R2025a). Each iteration involves simulating engine behavior at given input settings and

evaluating the objective and constraint functions, thereby guiding the solution towards an optimal parameter set that ensures regulatory compliance and performance efficiency.

To compute the weighted average of NO_x and HC emissions, the engine is simulated at four representative operating points, as defined by regulatory test cycles and guidelines. For each operating point, the NO_x and HC emissions are predicted using the Arrhenius-based chemical kinetics equations, which are parameterized through prior calibration. The resulting emission values are then substituted into the standard emissions-weighted average formula, which applies specific weighting factors to each operating condition to reflect their contribution to overall engine operation. This aggregated emission index is subsequently evaluated within the optimization loop, serving as a key component of the objective function or constraint evaluation, enabling the model to identify optimal parameter sets that comply with emission regulations while maintaining engine efficiency.

Upon completion of the optimization procedure, the optimal values for the Arrhenius correlation coefficients ARC1 and AERC1 are determined to be 0.9572 and 1.1524, respectively. These values represent the best fit parameters within the defined boundary conditions, ensuring accurate prediction of NO_x emissions based on the weighted target value.

After assigning the optimized values of ARC1 and AERC1 to the NO_x emissions sub-model within the WAVE simulation environment, the corresponding emissions of NO_x and HC are computed across the defined engine operating points. The simulation results, which reflect the updated kinetic behavior based on the tuned Arrhenius parameters, are presented in Table 3, illustrating the model's ability to accurately capture the emissions trends under varying load and speed conditions.

Table 3. Exhaust emissions results based on the optimized values of the Arrhenius equation.

Engine Speed (RPM)	Brake Power (kW)	NO_x Emissions (g/kWh)	NO_x Emissions (g/h)	HC Emissions (g/kWh)	HC Emissions (g/h)
2100	749	6.89	5164	0.100	74.85
1911	561.75	7.61	4277	0.097	54.44
1680	374.5	5.91	2215	0.100	37.26
1323	187.25	5.66	1061	0.106	19.93

At the rated speed of 2100 RPM, the engine delivers a maximum brake power of 749 kW. Under these conditions, the NO_x emissions are 6.89 g/kWh, resulting in a total hourly NO_x output of 5164 g/h. The HC emissions are 0.100 g/kWh, with a total of 74.85 g/h.

As the engine speed decreases to 1911 RPM, the brake power drops to 561.75 kW. Despite this reduction in output, the specific NO_x emissions increase to 7.61 g/kWh, which is close to the regulatory threshold. This rise can be explained by the fact that NO_x emissions in g/kWh are normalized against engine power output. Therefore, as power decreases, even a modest absolute emission rate can yield a higher value when expressed per unit of energy. Additionally, part-load operation typically results in lower air flow rates and increased in-cylinder temperatures, which promote thermal NO_x formation. Nevertheless, the total hourly NO_x output drops to 4277 g/h, consistent with the reduced fuel input and combustion energy. HC emissions also show a slight decline, with values of 0.097 g/kWh and 54.44 g/h, indicating stable combustion quality at this load point.

At 1680 RPM, with a brake power of 374.5 kW, the specific NO_x emissions decrease to 5.91 g/kWh, and the total output falls to 2215 g/h. HC emissions remain stable at 0.100 g/kWh, but the total HC output declines further to 37.26 g/h.

At the lowest operating point of 1323 RPM, the engine produces 187.25 kW. NO_x emissions continue to drop to 5.66 g/kWh and 1061 g/h, indicating improved NO_x control

at low loads. HC emissions slightly increase in specific terms to 0.106 g/kWh, but the total hourly emission is minimal at 19.93 g/h.

Importantly, none of the NO_x values at the individual operating points exceed the maximum limit set by the IMO Tier II regulation, which stipulates that the weighted average NO_x emissions across the four test modes must not exceed 7.7 g/kWh. This ensures that the engine meets the compliance criteria not only at full load but also across part-load conditions, as reflected in the simulation results. The optimization model successfully captures this behavior and guides the engine operation towards regulatory compliance while maintaining consistent performance.

4.3. Sensitivity Analysis

To investigate the individual influence of the Arrhenius correlation coefficients on NO_x formation, a sensitivity analysis is conducted by varying each parameter—ARC1 and AERC1—independently across a defined range while holding the other constant. This approach allows for isolating the impact of each coefficient on the predicted NO_x emissions, thereby providing deeper insight into the model's sensitivity and the relative importance of each term in the extended Zeldovich mechanism. The analysis supports the identification of the most influential parameter for calibration and optimization tasks.

Figure 5 presents a sensitivity analysis showing the effect of the ARC1 on NO_x emissions (g/kWh) at four different engine load conditions: 100% (L100), 75% (L75), 50% (L50), and 25% (L25). NO_x emissions increase consistently with higher values of ARC1 across all load conditions. This aligns with the role of ARC1 in amplifying the reaction rate for thermal NO formation within the extended Zeldovich mechanism. At any given ARC1 value, NO_x emissions are highest at higher loads and decrease with lower engine loads. This is expected, as higher engine loads typically result in higher peak in-cylinder temperatures, promoting NO_x formation due to more favorable thermodynamic conditions. The slope of each curve indicates the sensitivity of NO_x emissions to changes in ARC1.

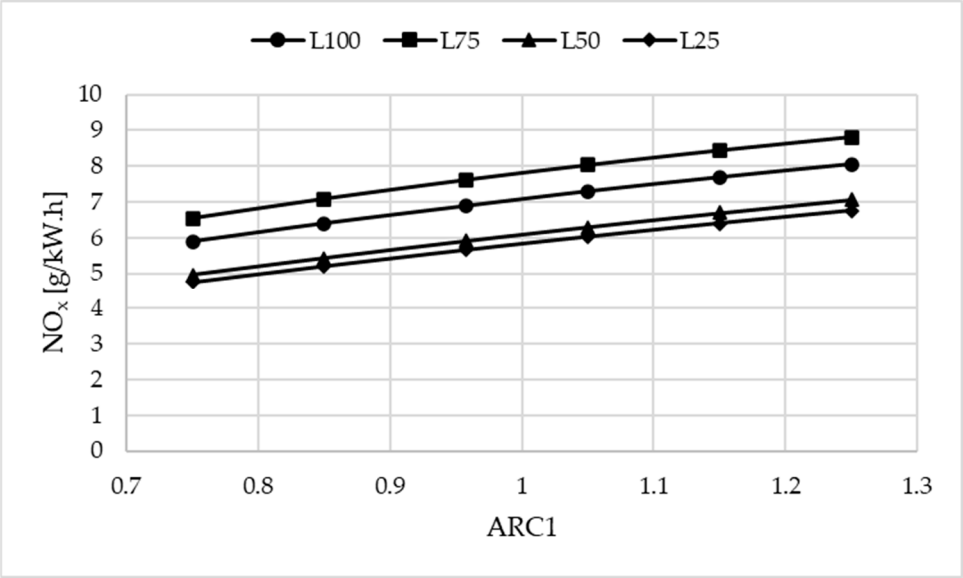

Figure 5. Variation in NO_x emissions with different values of ARC1 at various engine load conditions, with AERC1 held constant.

The steepest slope appears at higher loads, showing that NO_x formation is more sensitive to ARC1 at higher loads due to more pronounced combustion temperatures. Conversely, at L25, the response is more gradual, reflecting a less temperature-sensitive NO_x generation regime at low load. Across the ARC1 range (0.75 to 1.25), NO_x emissions

vary by approximately 2–3 g/kWh at each load level. This demonstrates that ARC1 tuning has a significant impact on emission estimates and must be carefully calibrated to reflect real engine behavior.

Figure 6 shows the results of a sensitivity analysis of the exponent multiplier (AERC1) on NO_x emissions (g/kWh) at the four different engine load conditions (L100, L75, L50, and L25), similar to the previous figure. NO_x emissions decrease significantly as AERC1 increases from 0.75 to 1.25 across all load conditions. This inverse relationship indicates that increasing the temperature exponent reduces the rate of NO formation as calculated by the extended Zeldovich mechanism, likely due to enhanced temperature sensitivity dampening the effective reaction rate under certain thermal ranges. Compared to ARC1, the sensitivity of NO_x emissions to AERC1 is more pronounced. For instance, increasing AERC1 from 0.75 to 1.25 reduces NO_x from over 20 g/kWh to around 3 g/kWh. This suggests AERC1 has a stronger impact on NO_x output and must be carefully controlled during calibration. The relative position of the curves suggests that at any AERC1 value, NO_x emissions increase with engine load—likely due to higher in-cylinder temperatures at higher loads. However, the rate of decrease in NO_x with increasing AERC1 is fairly consistent across the different load levels. The curves exhibit a nonlinear decay, becoming steeper at higher AERC1 values, indicating a compounding effect of the exponent multiplier on NO_x suppression at higher values.

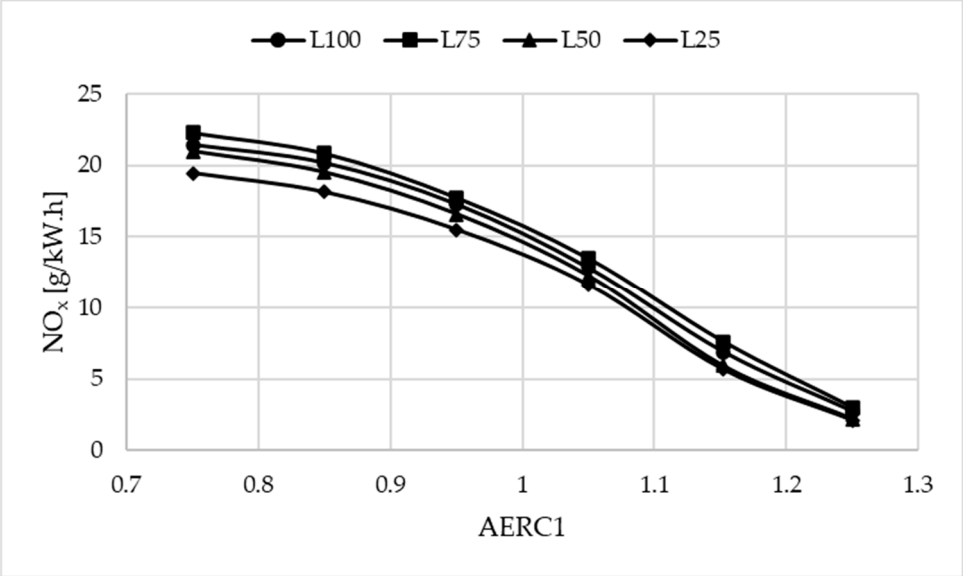

Figure 6. Variation of NO_x emissions with different values of AERC1 at various engine load conditions, with ARC1 held constant.

The above figures confirm that ARC1 is a critical parameter influencing NO_x emission predictions, especially at high engine loads. Therefore, precise calibration of ARC1 is essential for ensuring accurate and load-responsive emissions modeling in marine engine simulations. However, the AERC1 is a highly sensitive and influential parameter in NO_x formation modeling. Even small changes in its value lead to large variations in predicted emissions. Its effect is more significant than that of ARC1, emphasizing its critical role in the calibration of the extended Zeldovich mechanism for accurate NO_x prediction across all engine loads.

5. Conclusions and Future Trends

This study proposed and successfully implemented an efficient and practical calibration strategy for NO_x emissions modeling in a high-speed dual-fuel marine diesel engine.

The methodology combines 1D engine simulations using WAVE 2025.1 with a nonlinear optimization routine (fmincon in MATLAB R2025a), offering a systematic framework to fine-tune the extended Zeldovich mechanism by optimizing key Arrhenius equation parameters (ARC1 and AERC1).

A key strength of the approach lies in its ability to achieve accurate NO_x predictions without requiring extensive experimental datasets at every operating point, thus significantly reducing the time and resource demands typically associated with engine emissions calibration. Instead, the method leverages manufacturer-supplied emissions data and empirical trends to construct an integrated NO_x and HC emission map. This simplification enhances the applicability of the model in early-stage engine design, performance simulation, and feasibility studies involving alternative fuels or dual-fuel operation.

The calibration process successfully achieved a weighted combined NO_x and HC emission output of 7.2 g/kWh, aligned with IMO Tier II regulatory thresholds. Simulations at four representative engine loads from the IMO E3 test cycle demonstrated consistent compliance, and results confirmed that the emissions performance remains within allowable limits even under part-load conditions, where thermal NO_x formation typically increases.

A notable limitation of the proposed calibration methodology is the absence of direct experimental NO_x measurements at individual engine operating points. However, the model is capable of computing NO_x emissions at each operating condition, using simulation-based predictions, with a degree of uncertainty. This approach significantly reduces the need for extensive experimental testing and supports practical early-stage assessments, particularly when detailed measurement data are unavailable. By relying on manufacturer-supplied emissions data as reference targets, the methodology enables efficient calibration while maintaining acceptable predictive accuracy. Future work will incorporate direct experimental data to further enhance the physical consistency and reliability of the NO_x predictions.

Furthermore, the calibrated model provides a reliable foundation for the following:

- Conducting parametric studies involving injection timing, turbocharger settings, or fuel blending ratios;
- Supporting retrofit evaluations of existing engines transitioning to dual-fuel configurations;
- Feeding real-time prediction systems or digital twins for onboard emission monitoring and control;
- Serving as a surrogate model for broader multi-objective optimization tasks aimed at balancing power output, fuel consumption, and environmental compliance.

Overall, this study delivers a computationally efficient and scalable emissions modeling approach that bridges the gap between physical accuracy and engineering practicality. It enables marine engineers and researchers to integrate NO_x modeling directly into engine performance simulations, optimization workflows, and regulatory validation procedures—paving the way for cleaner, smarter propulsion system development in line with global maritime decarbonization targets.

Author Contributions: Conceptualization, M.T.; methodology, M.T.; formal analysis, M.T.; investigation, M.T.; writing—original draft preparation, M.T.; writing—review and editing, M.T. and E.B. All authors have read and agreed to the published version of the manuscript.

Funding: The authors affiliated with Maritime Safety Research Centre (MSRC) greatly acknowledge the financial support by the MSRC sponsors DNV and RCG. The opinions expressed herein are those of the authors and should not be construed to reflect the views of EU, DNV, RCG.

Institutional Review Board Statement: Not applicable.

Informed Consent Statement: Not applicable.

Data Availability Statement: The data presented in this study are available on request from the corresponding author.

Conflicts of Interest: The authors declare no conflicts of interest.

Abbreviations

1D	One dimensional
3D	Three dimensional
A	Pre-exponential constant
AERC1	Exponent multiplier
AFR	Air-fuel ratio
AI	Artificial intelligence
ARC1	Pre-exponent multiplier
BSFC	Brake-specific fuel consumption
BTDC	Before top dead center
CFD	Computational fluid dynamics
CO	Carbon monoxide
CO_2	Carbon dioxide
ECA	Emission Control Area
EGR	Exhaust gas recirculation
f	Fitness function
FMEP	Friction mean effective pressure
GHG	Greenhouse gas
H	Hydrogen atom
HC	Unburned hydrocarbon
HFO	Heavy fuel oil
IMO	International Maritime Organization
Inj_{Dur}	Injection duration
k-ε RNG	Renormalization Group
LNG	Liquefied natural gas
MDO	Marine diesel oil
ML	Machine learning
n	Number of simulated cases
N	Nitrogen atom
N_2	Nitrogen
NO	Nitric oxide
NO_2	Nitrogen dioxide
NO_x	Nitrogen oxides
O	Oxygen atom
O_2	Oxygen
P_B	Brake power
PM	Particulate matter
RPM	Engine speed
SCR	Selective catalytic reduction
SO_x	Sulfur oxides
T	Burned-zone temperature
T_a	Activation temperature
w	Weighting factor

References

1. Tadros, M.; Ventura, M.; Guedes Soares, C. Review of the IMO Initiatives for Ship Energy Efficiency and Their Implications. *J. Mar. Sci. Appl.* **2023**, *22*, 662–680. [CrossRef]
2. Hautala, S.; Mikulski, M.; Söderäng, E.; Storm, X.; Niemi, S. Toward a digital twin of a mid-speed marine engine: From detailed 1D engine model to real-time implementation on a target platform. *Int. J. Engine Res.* **2022**, *24*, 4553–4571. [CrossRef]
3. Sawant, P.; Warstler, M.; Bari, S. Exhaust Tuning of an Internal Combustion Engine by the Combined Effects of Variable Exhaust Pipe Diameter and an Exhaust Valve Timing System. *Energies* **2018**, *11*, 1545. [CrossRef]
4. Lamas, M.I.; Rodríguez, J.d.D.; Castro-Santos, L.; Carral, L.M. Effect of multiple injection strategies on emissions and performance in the Wärtsilä 6L 46 marine engine. A numerical approach. *J. Clean. Prod.* **2019**, *206*, 1–10. [CrossRef]
5. Bertram, A.M.; Zhang, Q.; Kong, S.-C. A novel particle swarm and genetic algorithm hybrid method for diesel engine performance optimization. *Int. J. Engine Res.* **2016**, *17*, 732–747. [CrossRef]
6. Wu, Z.; Rutland, C.J.; Han, Z. Numerical optimization of natural gas and diesel dual-fuel combustion for a heavy-duty engine operated at a medium load. *Int. J. Engine Res.* **2018**, *19*, 682–696. [CrossRef]
7. Shailaja, M.; Sita Rama Raju, A.V. Neural Network—Based Diesel Engine Emissions Prediction for Variable Injection Timing, Injection Pressure, Compression Ratio and Load Conditions. In *Emerging Trends in Electrical, Communications and Information Technologies*; Springer: Singapore, 2017.
8. Tadros, M.; Ventura, M.; Guedes Soares, C. Optimization procedure to minimize fuel consumption of a four-stroke marine turbocharged diesel engine. *Energy* **2019**, *168*, 897–908. [CrossRef]
9. Liu, J.; Wang, J.; Zhao, H. Optimization of the injection parameters and combustion chamber geometries of a diesel/natural gas RCCI engine. *Energy* **2018**, *164*, 837–852. [CrossRef]
10. Wang, H.; Gan, H.; Theotokatos, G. Parametric investigation of pre-injection on the combustion, knocking and emissions behaviour of a large marine four-stroke dual-fuel engine. *Fuel* **2020**, *281*, 118744. [CrossRef]
11. Stoumpos, S.; Theotokatos, G. Multiobjective Optimisation of a Marine Dual Fuel Engine Equipped with Exhaust Gas Recirculation and Air Bypass Systems. *Energies* **2020**, *13*, 5021. [CrossRef]
12. Lu, D.; Theotokatos, G.; Zhang, J.; Zeng, H.; Cui, K. Parametric investigation of a large marine two-stroke diesel engine equipped with exhaust gas recirculation and turbocharger cut out systems. *Appl. Therm. Eng.* **2022**, *200*, 117654. [CrossRef]
13. Lu, D.; Theotokatos, G.; Zhang, J.; Zeng, H.; Cui, K. Comparative Assessment and Parametric Optimisation of Large Marine Two-Stroke Engines with Exhaust Gas Recirculation and Alternative Turbocharging Systems. *J. Mar. Sci. Eng.* **2022**, *10*, 351. [CrossRef]
14. Tang, X.; Wang, P.; Zhang, Z.; Zhang, F.; Shi, L.; Deng, K. Effects of high-pressure and donor-cylinder exhaust gas recirculation on fuel economy and emissions of marine diesel engines. *Fuel* **2022**, *309*, 122226. [CrossRef]
15. Karabektas, M. The effects of turbocharger on the performance and exhaust emissions of a diesel engine fuelled with biodiesel. *Renew. Energy* **2009**, *34*, 989–993. [CrossRef]
16. Tadros, M.; Ventura, M.; Guedes Soares, C. A nonlinear optimization tool to simulate a marine propulsion system for ship conceptual design. *Ocean Eng.* **2020**, *210*, 107417. [CrossRef]
17. Tadros, M.; Ventura, M.; Guedes Soares, C. Assessment of marine Genset performance with biodiesel fuel using the double-Wiebe function. In *Trends in Maritime Technology and Engineering*; Guedes Soares, C., Santos, T.A., Eds.; Taylor & Francis Group: London, UK, 2022; pp. 545–551.
18. Karatuğ, Ç.; Ceylan, B.O.; Ejder, E.; Arslanoğlu, Y. Investigation and Examination of LNG, Methanol, and Ammonia Usage on Marine Vessels. In *Decarbonization of Maritime Transport*; Zincir, B., Shukla, P.C., Agarwal, A.K., Eds.; Springer Nature: Singapore, 2023; pp. 65–85.
19. Mohd Noor, C.W.; Noor, M.M.; Mamat, R. Biodiesel as alternative fuel for marine diesel engine applications: A review. *Renew. Sustain. Energy Rev.* **2018**, *94*, 127–142. [CrossRef]
20. Witcover, J.; Williams, R.B. Comparison of "Advanced" biofuel cost estimates: Trends during rollout of low carbon fuel policies. *Transp. Res. D Transp. Environ.* **2020**, *79*, 102211. [CrossRef]
21. Zhang, B.; Jiang, Y.; Chen, Y. Research on Calibration, Economy and PM Emissions of a Marine LNG—Diesel Dual-Fuel Engine. *J. Mar. Sci. Eng.* **2022**, *10*, 239. [CrossRef]
22. Soni, D.K.; Gupta, R. Optimization of methanol powered diesel engine: A CFD approach. *Appl. Therm. Eng.* **2016**, *106*, 390–398. [CrossRef]
23. Balcombe, P.; Staffell, I.; Kerdan, I.G.; Speirs, J.F.; Brandon, N.P.; Hawkes, A.D. How can LNG-fuelled ships meet decarbonisation targets? An environmental and economic analysis. *Energy* **2021**, *227*, 120462. [CrossRef]
24. Tadros, M.; Ventura, M.; Guedes Soares, C. Review of current regulations, available technologies, and future trends in the green shipping industry. *Ocean Eng.* **2023**, *280*, 114670. [CrossRef]
25. Tadros, M.; Ventura, M.; Guedes Soares, C. Optimization of the performance of marine diesel engines to minimize the formation of SOx emissions. *J. Mar. Sci. Appl.* **2020**, *19*, 473–484. [CrossRef]

26. Balcombe, P.; Brierley, J.; Lewis, C.; Skatvedt, L.; Speirs, J.; Hawkes, A.; Staffell, I. How to decarbonise international shipping: Options for fuels, technologies and policies. *Energy Convers. Manag.* **2019**, *182*, 72–88. [CrossRef]
27. Mukherjee, A.; Bruijnincx, P.; Junginger, M. Techno-economic competitiveness of renewable fuel alternatives in the marine sector. *Renew. Sustain. Energ. Rev.* **2023**, *174*, 113127. [CrossRef]
28. Zhao, J.; Wei, Q.; Wang, S.; Ren, X. Progress of ship exhaust gas control technology. *Sci. Total Environ.* **2021**, *799*, 149437. [CrossRef]
29. Nemmour, A.; Inayat, A.; Janajreh, I.; Ghenai, C. Green hydrogen-based E-fuels (E-methane, E-methanol, E-ammonia) to support clean energy transition: A literature review. *Int. J. Hydrogen Energy* **2023**, *48*, 29011–29033. [CrossRef]
30. El-Gohary, M.M.; Seddiek, I.S.; Salem, A.M. Overview of alternative fuels with emphasis on the potential of liquefied natural gas as future marine fuel. *Proc. Inst. Mech. Eng. Part M* **2015**, *229*, 365–375.
31. Heywood, J.B. *Internal Combustion Engine Fundamentals*; McGraw-Hill: New York, NY, USA, 1988.
32. Savva, N.S.; Hountalas, D.T. Evolution and application of a pseudo-multi-zone model for the prediction of NOx emissions from large-scale diesel engines at various operating conditions. *Energy Convers. Manag.* **2014**, *85*, 373–388. [CrossRef]
33. Cho, H.; Fulton, B.; Upadhyay, D.; Brewbaker, T.; van Nieuwstadt, M. In-cylinder pressure sensor–based NOx model for real-time application in diesel engines. *Int. J. Engine Res.* **2018**, *19*, 293–307. [CrossRef]
34. Özgül, E.; Bedir, H. Fast NOx emission prediction methodology via one-dimensional engine performance tools in heavy-duty engines. *Adv. Mech. Eng.* **2019**, *11*, 1687814019845954. [CrossRef]
35. Berni, F.; Pessina, V.; Teodosio, L.; d'Adamo, A.; Borghi, M.; Fontanesi, S. An integrated 0D/1D/3D numerical framework to predict performance, emissions, knock and heat transfer in ICEs fueled with NH_3–H_2 mixtures: The conversion of a marine Diesel engine as case study. *Int. J. Hydrogen Energy* **2024**, *50*, 908–938. [CrossRef]
36. Neshat, E.; Honnery, D.; Saray, R.K. Multi-zone model for diesel engine simulation based on chemical kinetics mechanism. *Appl. Therm. Eng.* **2017**, *121*, 351–360. [CrossRef]
37. Raptotasios, S.I.; Sakellaridis, N.F.; Papagiannakis, R.G.; Hountalas, D.T. Application of a multi-zone combustion model to investigate the NOx reduction potential of two-stroke marine diesel engines using EGR. *Appl. Energy* **2015**, *157*, 814–823. [CrossRef]
38. Cuper-Przybylska, D.; Nguyen, V.N.; Nam, C.D.; Kowalski, J. High Quality Multi-Zone and 3D CFD Model of Combustion in Marine Diesel Engine Cylinder. *Pol. Marit. Res.* **2023**, *30*, 61–67. [CrossRef]
39. Jo, K.-S.; Kong, K.-J.; Han, S.-H. Comparative Analysis of Combustion Characteristics and Emission Formation in Marine Diesel Engines Using Biofuels: Chemical Mechanism Analysis and Computational Fluid Dynamics Simulation. *J. Mar. Sci. Eng.* **2025**, *13*, 1098. [CrossRef]
40. Sun, X.; Liang, X.; Shu, G.; Lin, J.; Wang, Y.; Wang, Y. Numerical investigation of two-stroke marine diesel engine emissions using exhaust gas recirculation at different injection time. *Ocean Eng.* **2017**, *144*, 90–97. [CrossRef]
41. Lamas, M.I.; Rodríguez, C.G. Numerical model to study the combustion process and emissions in the Wärtsilä 6L 46 four-stroke marine engine. *Pol. Marit. Res.* **2013**, *20*, 61–66. [CrossRef]
42. Şener, R.; Gül, M.Z. Optimization of the combustion chamber geometry and injection parameters on a light-duty diesel engine for emission minimization using multi-objective genetic algorithm. *Fuel* **2021**, *304*, 121379. [CrossRef]
43. Karvounis, P.; Theotokatos, G.; Patil, C.; Xiang, L.; Ding, Y. Parametric investigation of diesel–methanol dual fuel marine engines with port and direct injection. *Fuel* **2025**, *381*, 133441. [CrossRef]
44. Liu, L.; Wu, Y.; Wang, Y. Numerical investigation on the combustion and emission characteristics of ammonia in a low-speed two-stroke marine engine. *Fuel* **2022**, *314*, 122727. [CrossRef]
45. Karjalainen, P.; Teinilä, K.; Kuittinen, N.; Aakko-Saksa, P.; Bloss, M.; Vesala, H.; Pettinen, R.; Saarikoski, S.; Jalkanen, J.-P.; Timonen, H. Real-world particle emissions and secondary aerosol formation from a diesel oxidation catalyst and scrubber equipped ship operating with two fuels in a SECA area. *Environ. Pollut.* **2022**, *292*, 118278. [CrossRef]
46. Du, S.; Gong, M.; Wang, Q. Development of a NOx Calculation Model for Low-Speed Marine Diesel Engines Based on Soft Measurement Technology. *Appl. Sci.* **2023**, *13*, 6373. [CrossRef]
47. Wang, K.; Yan, X.; Yuan, Y.; Li, F. Real-time optimization of ship energy efficiency based on the prediction technology of working condition. *Transp. Res. D Trans. Environ.* **2016**, *46*, 81–93. [CrossRef]
48. Mocerino, L.; Guedes Soares, C.; Rizzuto, E.; Balsamo, F.; Quaranta, F. Validation of an Emission Model for a Marine Diesel Engine with Data from Sea Operations. *J. Mar. Sci. Appl.* **2021**, *20*, 534–545. [CrossRef]
49. Castresana, J.; Gabiña, G.; Martin, L.; Basterretxea, A.; Uriondo, Z. Marine diesel engine ANN modelling with multiple output for complete engine performance map. *Fuel* **2022**, *319*, 123873. [CrossRef]
50. MAN Diesel & Turbo. *MAN Dual Fuel Marine Engine: Sustainable Hydrogen-Diesel Solution*; MAN Diesel & Turbo: Augsburg, Germany, 2022; Available online: https://www.man.eu/engines/en/products/marine/man-dual-fuel-marine-engine.html (accessed on 15 April 2023).

51. MAN Diesel & Turbo. *Technical Data Sheet: Marine Diesel Engine D2862 LE428*; MAN Diesel & Turbo: Augsburg, Germany, 2022; Available online: https://www.man.eu/ntg_media/media/content_medien/doc/man_engines_1/produkte/marine_1/Marine_DualFuel_EN.pdf (accessed on 15 April 2023).
52. Realis Simulation. *WAVE 2025.1 Help System*; Realis Simulation: Shoreham-by-Sea, UK, 2025.
53. The MathWorks Inc. Fmincon. 2016. Available online: https://www.mathworks.com/help/optim/ug/fmincon.html (accessed on 2 June 2017).
54. DieselNet. Emission Standards. Available online: https://dieselnet.com/standards/us/marine.php#cat3 (accessed on 4 July 2016).
55. NeRF. *NOx Technical Code on Control of Emission of Nitrogen Oxides from Marine Diesel Engines (MEPC.132(53))*; NeRF: Springfield, VA, USA; Available online: https://puc.overheid.nl/nsi/doc/PUC_2419_14/1/ (accessed on 4 March 2020).
56. Tadros, M. Engine Optimization Model for Accurate Prediction of Friction Model in Marine Dual-Fuel Engine. *Algorithms* **2025**, *18*, 415. [CrossRef]
57. Chen, S.K.; Flynn, P.F. Development of Single Cylinder Compression Ignition Research Engine. SAE Technical Paper 650733. 1965. Available online: https://www.sae.org/publications/technical-papers/content/650733/ (accessed on 17 August 2025).
58. Tadros, M.; Ventura, M.; Guedes Soares, C. Assessment of the performance and the exhaust emissions of a marine diesel engine for different start angles of combustion. In *Maritime Technology and Engineering 3*; Guedes Soares, C., Santos, T.A., Eds.; Taylor & Francis Group: London, UK, 2016; pp. 769–775.
59. Tadros, M.; Ventura, M.; Guedes Soares, C. Data Driven In-Cylinder Pressure Diagram Based Optimization Procedure. *J. Mar. Sci. Eng.* **2020**, *8*, 294. [CrossRef]

Disclaimer/Publisher's Note: The statements, opinions and data contained in all publications are solely those of the individual author(s) and contributor(s) and not of MDPI and/or the editor(s). MDPI and/or the editor(s) disclaim responsibility for any injury to people or property resulting from any ideas, methods, instructions or products referred to in the content.